A Focused Optically Transparent PVDF Transducer for Photoacoustic Microscopy

Cheng Fang, *Student Member, IEEE*, He Hu, *Member, IEEE*, and Jun Zou, *Senior Member, IEEE*

***Abstract*—This papers reports the development of a novel focused optically-transparent ultrasound transducer with a wide bandwidth for photoacoustic microscopy (PAM). It consists of a 9-μm-thick polyvinylidene fluoride (PVDF) film coated with Indium-tin oxide (ITO) and metal electrodes, which is laminated onto a concave glass lens. A new fabrication process was developed to ensure the formation of continuous ITO coatings on the curved transducer surface without fracturing. Both optical and acoustic experiments were conducted to characterize the performance of the transducer. The testing results show that the transducer has an optical transmittance of 60% (@ 532 nm), an acoustic center frequency of 24 MHz, and an acoustic bandwidth of 26 MHz. With an acoustic numerical aperture (NA) of 0.23, it provides a 0.13-mm acoustic focal spot and a 1.6-mm focal depth. For demonstration, a PAM setup was built for conducting PA imaging on different targets. In contrast to existing PAM systems, the use of the optically-transparent focused transducer allows a simpler and more compact configuration and easier alignment of the optical excitation and acoustic focal points. Such features are especially useful for the development of miniaturized PAM systems for handheld, wearable and even endoscopic applications.**

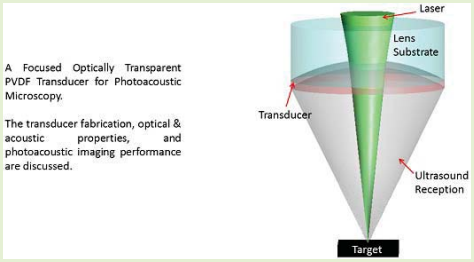

***Index Terms*— Photoacoustic microscopy, focused transparent ultrasound transducer, PVDF.**

I. Introduction

In THE past decade, photoacoustic microscopy (PAM) has emerged as a new hybrid imaging modality combining rich optical contrast with deep acoustic penetration (beyond the optical diffraction limit) [1], [2]. It can provide unique imaging capabilities that cannot be achieved with single optical or acoustic modality alone. To conduct PAM, an integrative imaging setup consisting of both optical and acoustic components is required. Their synergistic operation is essential for obtaining optimal imaging performance. Nevertheless, the optical and acoustic components in current PAM systems are not well compatible with each other. For example, the ultrasound transducers (for PA signal detection) consisting of optically-opaque material layers can completely block the light delivery to the target. On the other hand, the (glass) optical components (for light focusing and delivery) can reflect or scatter the PA signals due to their much higher acoustic impedance than the air or water. To address this issue, the current common practice is to route the optical and acoustic beams along different paths [3]–[5] (Figs. 1(a) and 1(b)). However, this approach could result in complex and bulky system configurations, difficulty in aligning the optical and acoustic beams, and also degradation of signal to noise ratio (SNR). Alternatively, a transmission-mode setup can be adopted to circumvent this problem, where the optical illumination and acoustic reception are conducted on the opposite sides of the target [6], [7] (Fig. 1(c)). However, it is not suitable for in-vivo applications due to the difficulty in delivering focused light through thick and optically-scattering biological tissues.

Recently, focused hollow or ring ultrasound transducers have been used [8], [9] to receive the PA signals while allowing the excitation light to pass through, which results in a much simpler and more compact imaging setup and easier alignment of the laser and ultrasound beams (Fig. 2(a)). However, with the center part of the transducer removed, the acoustic sensitivity and focusing capability of the transducer are compromised. More recently, flat or planar piezoelectric or optical ultrasound transducers made of optically transparent sensing and electrode materials have been developed for PAM (Fig. 2(b)) [10]–[17]. These transparent transducers can have adequate optical transmittance at the laser excitation wavelength and provide a complete sensing substrate for receiving the PA signal. However, without a well-defined acoustic focal point, these transducers do not provide an optimal detection

Manuscript received October 1, 2019; revised November 7, 2019; accepted November 7, 2019. Date of publication November 11, 2019; date of current version February 5, 2020. This work was supported in part by an award (1748161) from the National Science Foundation and in part by the Prematurity Research Center Grant from the March of Dimes Foundation. The associate editor coordinating the review of this article and approving it for publication was Prof. Marco Petrovich. *(Corresponding author: Cheng Fang.)*

The authors are with the Electrical and Computer Engineering Department, Texas A&M University College Station, College Station, TX 77843 USA (e-mail: fangchengok2007@tamu.edu).

Digital Object Identifier 10.1109/JSEN.2019.2952971

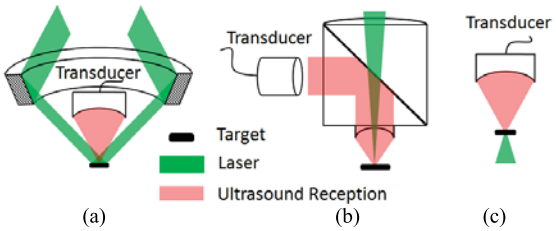

Fig. 1. (a) Acoustic-resolution (AR-) PAM setup with a ring-shaped mirror. (b) Optical-resolution (OR-) PAM setup with an optical-acoustic beam combiner formed by two isosceles prisms. (c) Transmission-mode PAM.

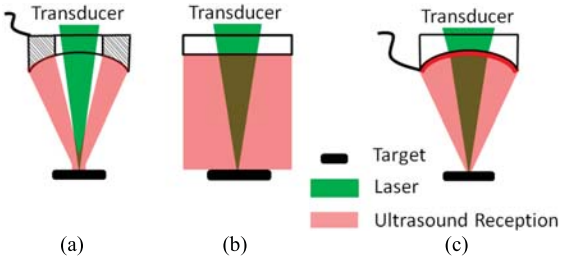

Fig. 2. (a) PAM setup with a hollow or ring-shaped transducer. (b) PAM setup with a flat or planar transparent transducer. (c) PAM setup with a focused transparent transducer.

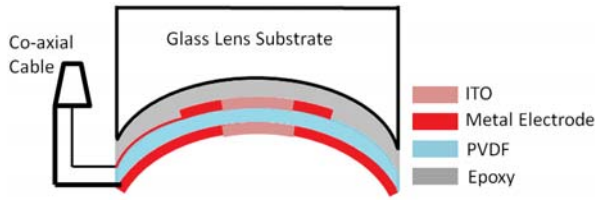

Fig. 3. Schematic of the focused transparent transducer design.

condition for the PA signals (typically a spherical wave emitting from the illumination point).

This paper reports the development of a new focused optically transparent PVDF (polyvinylidene fluoride) ultrasound transducer for PAM (Fig. 2(c)). Its optical and acoustic properties have been experimentally characterized. Using the focused transparent transducer, an optical-resolution PAM imaging setup has been built and imaging experiments have been conducted on different targets. The imaging results show that the focused transparent transducer is functional and practical for PAM. It could enable new PAM imaging systems with a simpler and more compact configuration and easier co-alignment and co-registration of the optical excitation and acoustic detection, which is especially useful for handheld, wearable and even endoscopic applications.

II. Transducer Design and Construction

The schematic design of the focused transparent PVDF transducer is shown in Fig. 3. It consists of a thin PVDF film coated with ITO (indium-tin oxide)/metal electrodes, which is laminated onto a concave glass lens. Typically, a piezoelectric transducer is composed of a stack of functional materials: the impedance matching layer, the piezoelectric layer, two electrode layers, and the backing layer. PVDF is chosen as the

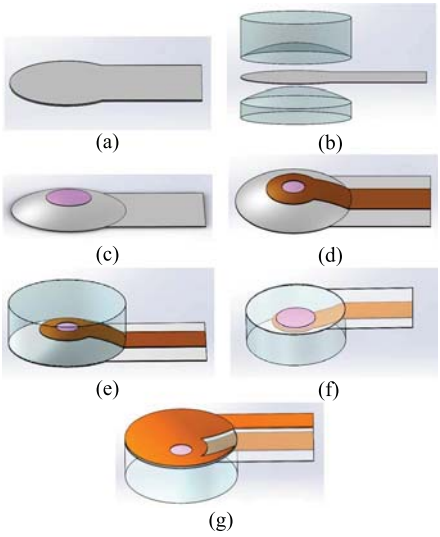

Fig. 4. Fabrication process flow of the focused transparent transducer.

piezoelectric layer due to its unique mechanical, optical and acoustic properties. First, it has high (>80%) optical transmittance over the wavelength range of 250 nm ~ 900 nm [18]. Second, it has low acoustic impedance and wide-band acoustic response, which make the matching and backing layers unnecessary to simplify the transducer structure. Due to the existence of a high concentration of micro particles for tuning their acoustic impedance, the matching (commonly by mixing micro particles into a polymer) and backing (usually high attenuated metal-loaded epoxy) [19]–[21] layers are usually optically opaque or scattering and therefore cannot be used for making the transparent transducers. Third, the mechanical flexibility of PVDF allows its lamination onto a spherical surface to form a shape-defined acoustic focal point without using an acoustic lens. Compared with focusing with an acoustic lens [20], [22], the molded focused transducer can provide better acoustic transmittance and wider bandwidth response.

ITO is a commonly used material of transparent electrodes with optical transmittance of >60% over 450 nm ~ 1100 nm [23]. Although it is much higher than many other transparent conductors, the conductivity of ITO is still limited especially for high-frequency applications at MHz and above. The high resistance of the ITO electrodes could significantly increase the signal loss and lower the bandwidth or the high cut-off frequency of the transducer. Therefore, depending on the diameter of the excitation laser beam, the area of the ITO electrode (i.e., the size of the transparent window) should be minimized. The non-transparent region can be covered with highly-conductive metal electrodes to reduce the overall resistance of the electrodes.

The detailed fabrication process flow of the focused transparent transducer is shown in Fig. 4. Firstly, a piece of flat 9-μm-thick PVDF film is trimmed with a film cutter (Fig. 4(a)). The PVDF film is compressed and stretched onto a mold consisting of a pair of convex and concave lenses with the same diameter and matched surface radius of curvature (Fig. 4(b)). Secondly, with two shadow masks, an ITO (400 nm thick) layer (Fig. 4(c)) and a chrome (15 nm)/ copper (200 nm)

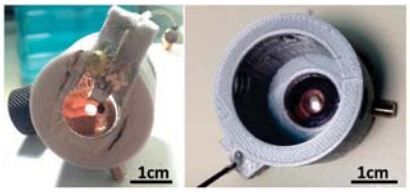

Fig. 5. Photographs of the (a) front side (b) back side of the fabricated focused transparent transducer mounted on a 3D-printed fixture.

layer (Fig. 4(d)) are deposited onto the convex side of the stretched PVDF film. Thirdly, the PVDF film is bonded onto the spherical surface of the concave glass (transmittance ≈ 90% over 350nm ∼ 2000nm [24]) lens with an UV epoxy (transmittance > 90% over 400nm ∼ 2000nm [25]) (Fig. 4(e)). Lastly, the electrode deposition process is repeated on the exposed side of the PVDF film (Fig. 4(f) and 4(g)). The surface of the PVDF film outside the transparent window at the center is coated with the chrome/copper layer, which serves as the ground electrode.

Fig. 5 shows a fabricated prototype of the focused transparent transducer. The overall diameter and the diameter of the center transparent window are 6 mm and 3 mm, respectively. The acoustic focal length set by the surface radius of curvature of the concave lens mold is 12.9 mm. The numerical aperture (NA) of the transducer is 0.23. A 50-ohm micro co-axial cable is connected to the Cr/Cu electrodes with conductive epoxy. The transducer is mounted onto a home-made plastic fixture to facilitate its attachment onto the objective lens of an optical microscope for testing.

III. Transducer Testing and Characterization

The optical and acoustic properties of the fabricated focused transparent PVDF transducer were characterized by using the setup shown in Fig. 6. A Q-switched 532-nm Nd:YAG laser (Elforlight, UK) triggered by a function generator (Keysight Technologies, USA) is used as the light source. The diameter of the output laser beam (pulse width < 1.8 ns) is expanded by a pair of lenses (Thorlabs, USA) and passed through a 50-μm pinhole (Thorlabs, USA). The laser beam is then passed through a beam splitter (Thorlabs, USA), reflected by a stationary mirror, and focused by a 10× microscope objective. The focused laser beam propagates through the focused transparent transducer onto the target of interests. A CCD camera is used to monitor the excitation region through the reverse path of the optical illumination. For acoustic testing, both the target and the front spherical surface of transducer were immersed in a water-filled petri dish for acoustic coupling. The petri dish was placed onto a computer-controlled X/Y motor stage (Physik Instrumente GmbH & Co. KG, Germany) and a manually-adjusted Z-axis stage (MPositioning, China).

First, the optical transmittance of the focused transparent PVDF transducer was characterized in air (without the target or petri dish). The repetition rate of the pulse laser was set to be 1 kHz. An optical power meter (Thorlabs, USA) was used to measure the average intensity of the light passing through the transducer. The light intensity after a bare concave glass

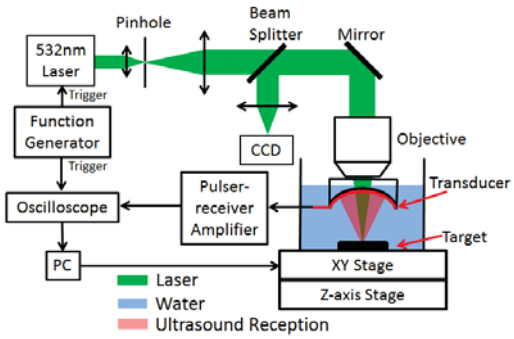

Fig. 6. Test setup for characterizing the optical and acoustic properties of focused transparent transducer.

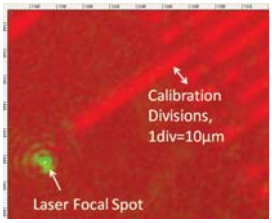

Fig. 7. Laser focal spot size measurement with a calibration glass slide.

lens was also measured as a reference. The optical transmittance of the focused transparent transducer was determined to be ∼60% at 532 nm. The influence on the optical focal spot size by the focused transparent transducer was characterized with a calibration glass slide placed in water. After travelling through the objective lens and a bare concave lens, the focal spot of the laser beam was estimated to be 3.6 μm (Fig. 7). It became 4.2 μm after going through the objective lens and the focused transparent transducer. Therefore, the focused transparent transducer does not significantly affect the transmission of the laser pulses for PA excitation.

An ultrasound pulse-echo testing was conducted to characterize the acoustic performance of the focused transparent transducer (with the pulsed laser turned off). The transducer was driven by a pulser-receiver (Olympus NDT, USA) with a 200 Hz repetition rate. The transmitted ultrasound pulses were incident onto a thick glass slide immersed in water. The reflected pulses propagated along the reversal path, and were received by the transducer and amplified by the preamplifier embedded in the pulser-receiver. The amplified pulse-echo signal (Fig. 8(a)) was captured and recorded with a digital oscilloscope (Tektronix Inc., USA) at a sampling rate of 5 GHz. The spectrum of the amplified pulse-echo signal is used to characterize the central frequency (f_c) and bandwidth (BW).

Fig. 8(b) shows the spectrum of the representative pulse-echo signal after applying water attenuation compensation [26] and low-pass noise filtering to remove high-frequency fluctuations, indicating an f_c and BW of 24 MHz and 26 MHz, respectively. The acoustic axial resolution is calculated as 14.81 μm. For comparison, a numerical simulation was conducted in the PiezoCAD® (Sonic Concepts, USA), which showed an f_c of 32 MHz (quarter-wavelength resonance) and a BW of 39 MHz. The measured f_c and BW of focused transparent transducer are somewhat lower than the simulated

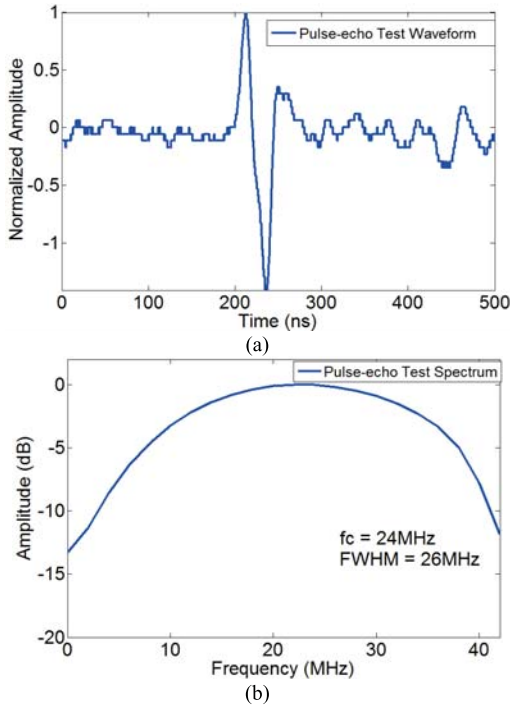

Fig. 8. (a) A representative echo signal. (b) Spectrum of the echo signal after low-pass noise filtering, indicating 24 MHz central frequency and 26 MHz −3 dB bandwidth.

TABLE I
MEASURED ACOUSTIC FOCAL SPOT AND PEAK AMPLITUDE AT DIFFERENT HEIGHT OF Z-AXIS STAGE

Height H (mm)	86.1	86.4	86.6	87.1	87.6	88.0	88.1
FWHM (mm)	0.17	0.15	0.13	0.13	0.13	0.15	0.17
Normalized Peak Amplitude	0.76	0.97	0.94	0.94	1	0.88	0.70

ones, due to three possible reasons. First, the pulse-echo signal could be broadened by the original ultrasound pulse overlapping with the reflected one after a round trip through epoxy. Second, the echo signal can be further broadened by the ultrasound wavefront with imperfect phase synchronization towards transducer spherical surface. Third, the higher resistance (especially in the ITO layer) and capacitance in the transducer can contribute to a low-pass RC filter to block high-frequency wave components.

To characterize the acoustic focal spot, the ultrasound pulse-echo testing was repeated with a 0.1-mm thick copper wire placed on the surface of a piece of 1% agar phantom as the target. The copper wire was scanned both horizontally and vertically around the (estimated) focal point of the transducer. The scanning range the horizontal direction is 0.25 mm with a fixed step size of 0.01 mm. The scanning range along the vertical direction is 2 mm with a variable step size (as H in Table I). At each height, the amplitude of the echo signal from the copper wire was recorded and normalized (Fig. 9). The FWHM (full width at half maximum) value of the Gaussian-fitted amplitude profile was used to determine

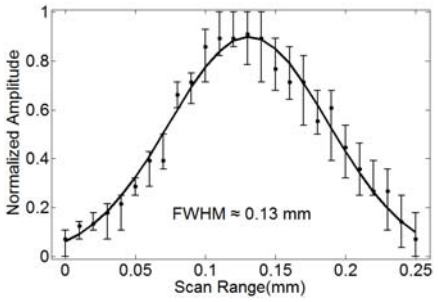

Fig. 9. A Gaussian-fitted profile of the echo signal amplitude across the scanning range.

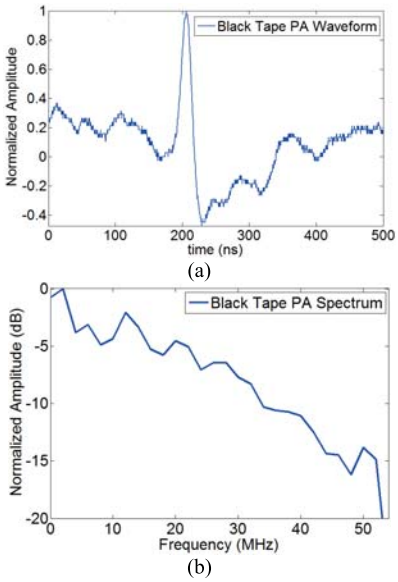

Fig. 10. (a) A representative PA signal from a black tape target. (b) The frequency spectrum of the PA signal.

the corresponding acoustic beam diameter. After repeating the horizontal scan at different height, the transducer acoustic focal spot was determined by the minimal FWHM, and the acoustic depth of focus was estimated by the height range with a relatively small FWHM. As listed in Table I, the acoustic focal spot size and focal depth of the focused transparent transducer were determined to be 0.13 mm and 1.6 mm, respectively.

IV. PAM EXPERIMENT AND RESULTS

A. PAM Imaging Setup

The PAM imaging setup with the focused transparent transducer is similar with the one used for the optical and acoustic testing (see Fig. 6), except that the pulse-receiver and oscilloscope were replaced with a homemade pre-amplifier and a data-acquisition (DAQ) card (Alarzar Tech, Canada). The optical and acoustic foci were firstly aligned together by adjusting the Z-axis stage to maximize the acoustic detection sensitivity. The photoacoustic signal received by the focused transparent transducer was amplified by 26 dB and sampled by the DAQ card at 250 MHz triggered by the function generator. The imaging target was continuously scanned on the X/Y

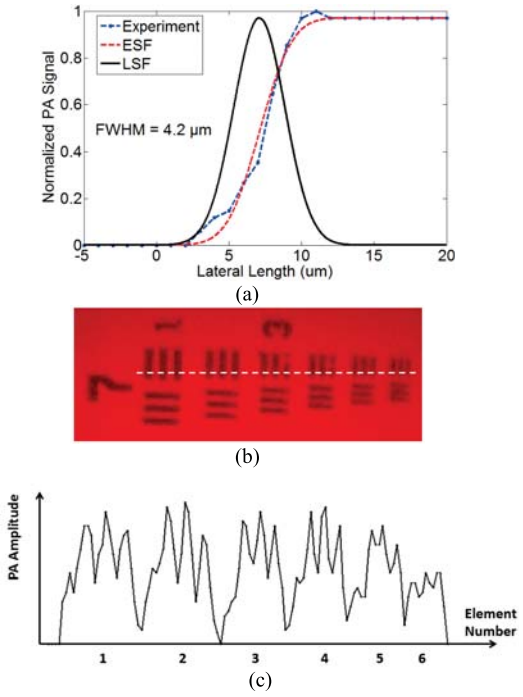

Fig. 11. (a) The FWHM of the LSF derived from ESF. (b) The photograph of the No. 7 elements on a resolution target, with the white dashed line indicating the scanning path. (c) The correponding cross-sectional PA profile.

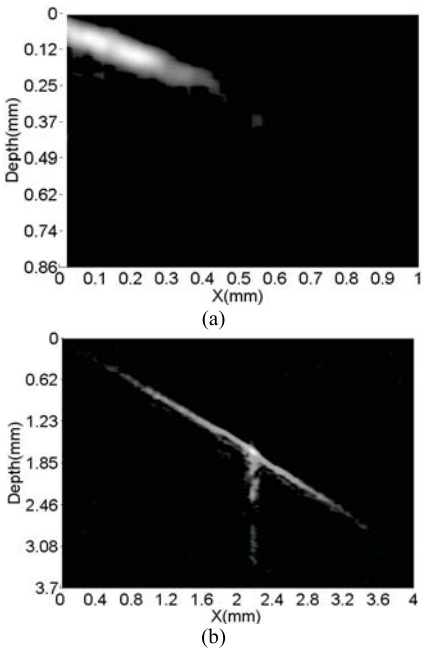

Fig. 12. B-mode PA image of (a) an ink-coated tungsten wire inserted in chicken breast and (b) an ink-coated needle inserted in 1% agar phantom.

stage, while PA signal was collected by DAQ card. Fig. 10(a) and Fig. 10(b) show a representative PA signal received from a black tape target and its frequency spectrum.

B. Lateral Resolution

The lateral resolution of the PAM imaging setup with the focused transparent transducer was characterized by measuring the full width at half maximum (FWHM) of the corresponding line spread function (LSF), which is the derivative of the edge spread function (ESF) [9]. The edge of a square Cr pattern on a USAF resolution target (Thorlabs, USA) was imaged, and the PA amplitude profile across the edge was fitted by the error function to compute the ESF and LSF, indicating the lateral resolution around 4.2 μm (Fig. 11(a)), which is comparable with those reported in previous works [4], [5], [8] and somewhat larger than the theoretical diffraction-limited focal spot size of 1.8 μm (for an optical wavelength of 532nm, a focal length of 20mm, and a beam diameter of 7.5 mm). Six groups of No. 7 line patterns on the resolution target were also scanned along the white dashed line shown in Fig. 11(b). Their cross-sectional PA profile is shown in Fig. 11(c). The smallest group of line patterns has a spatial frequency of 228 line-pairs/mm (corresponding to an FWHM resolution of 4.39 μm). They can be clearly resolved by the PAM imaging setup, which verifies the previously-determined lateral resolution.

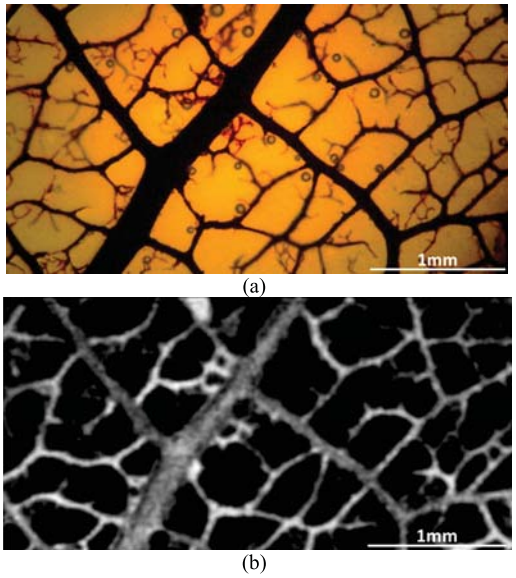

Fig. 13. (a) The optical photograph of the the black leaf skeleton phantom with a size of 4 × 2 mm^2. (b) PAM image of the black leaf skeleton.

C. Imaging Depth

The maximum penetration of the PAM imaging setup with the focused transparent transducer was characterized. A 240-μm-diameter tungsten wire coated with black ink was inserted into a thick piece of chicken breast at an oblique angle. With 100-nJ pulse energy, the PAM imaging setup can clearly image the tungsten wire down to around 0.3 mm beneath the surface (Fig. 12(a)). This relatively shallow depth is mainly limited by the strong optical absorption and scattering in chicken breast at 532 nm. To estimate the imaging depth in a more clear tissue, 1% agar (Sigma-Aldrich, USA) phantom was prepared and a 440-μm-diameter needle coated with black ink was inserted obliquely. As shown in Fig. 12(b), the PAM imaging setup can clearly image the needle down to 2.7 mm beneath the surface. Some artifacts exist at x = 2.2 mm, which is due to the acoustic resonance within needle caused by the sharply focused excitation.

D. Imaging Results

To demonstrate the 2D PAM imaging, a black leaf skeleton laminated on a glass substrate with epoxy was used as the imaging target (Fig. 13(a)). A total area of 4×2 mm^2 was scanned with a step size of 5 μm $\times$ 5 μm. At each location, the PA signals were averaged by 16 times to improve the signal-to-noise ratio (SNR) to around 15.2 dB. The PA image was reconstructed based on signal amplitude at each location, corresponding to the grayscale value of pixel. The reconstructed PA image is shown in Fig. 13(b). Most branches of the leaf skeleton phantom are resolved clearly. There exist some variations in the PA signal strength across the image, which would be due to height variations caused by the topographic features of the leaf skeleton branches. The same transducer has been used for months after fabrication without apparent degradation, indicating excellent durability.

V. Conclusions

In summary, a new focused optically transparent PVDF ultrasound transducer has been designed, fabricated and characterized and its application in PAM imaging has been demonstrated. The focused transparent transducer combines the advantages of the focused hollow and flat transparent transducers. It offers not only good optical transmittance allowing the excitation light to directly pass through, but also full aperture and well-defined acoustic focus for receiving the PA signal. Such capabilities could be used to enable a simpler and more compact PAM system configuration with optimal detection condition for the PA signals. Compared with existing (commercial) transducers used in PAM, the demonstrated focused transparent transducer still has lower sensitivity, which is mainly due to some limitations in the available materials, design and fabrication processes, such as low NA, high resistivity of ITO, and possible impedance mismatch between the transducer and amplifier. In future, more efforts will be made to address these issues to improve the transducer sensitivity.

References

[1] L. V. Wang, *Photoacoustic Imaging and Spectroscopy*. Boca Raton, FL, USA: CRC Press, 2009.

[2] L. V. Wang and J. Yao, "A practical guide to photoacoustic tomography in the life sciences," *Nature Methods*, vol. 13, no. 8, p. 627, Aug. 2016.

[3] K. Maslov, G. Stoica, and L. V. Wang, "*In vivo* dark-field reflection-mode photoacoustic microscopy," *Opt. Lett.*, vol. 30, no. 6, pp. 625–627, 2005.

[4] K. Maslov, H. F. Zhang, S. Hu, and L. V. Wang, "Optical-resolution photoacoustic microscopy for *in vivo* imaging of single capillaries," *Opt. Lett.*, vol. 33, no. 9, pp. 929–931, 2008.

[5] S. Hu, P. Yan, K. Maslov, J.-M. Lee, and L. V. Wang, "Intravital imaging of amyloid plaques in a transgenic mouse model using optical-resolution photoacoustic microscopy," *Opt. Lett.*, vol. 34, no. 24, pp. 3899–3901, 2009.

[6] Y. Wang *et al.*, "Fiber-laser-based photoacoustic microscopy and melanoma cell detection," *J. Biomed. Opt.*, vol. 16, no. 1, 2011, Art. no. 011014.

[7] J. Yao, L. Wang, C. Li, C. Zhang, and L. V. Wang, "Photoimprint photoacoustic microscopy for three-dimensional label-free subdiffraction imaging," *Phys. Rev. Lett.*, vol. 112, no. 1, 2014, Art. no. 014302.

[8] T. Wang *et al.*, "Multiparametric photoacoustic microscopy of the mouse brain with 300-kHz A-line rate," *Neurophotonics*, vol. 3, no. 4, 2016, Art. no. 045006.

[9] B. Lan *et al.*, "High-speed widefield photoacoustic microscopy of small-animal hemodynamics," *Biomed. Opt. Express*, vol. 9, no. 10, pp. 4689–4701, 2018.

[10] G. W. Brodie, Y. Qiu, S. Cochran, G. C. Spalding, and M. P. Macdonald, "Optically transparent piezoelectric transducer for ultrasonic particle manipulation," *IEEE Trans. Ultrason., Ferroelectr., Freq. Control*, vol. 61, no. 3, pp. 389–391, Mar. 2014.

[11] T. Hata, Y. Sato, Y. Nagai, and T. Hada, "Photoacoustic measurement of CdS by transparent transducer method," *Jpn. J. Appl. Phys.*, vol. 23, no. S1, p. 75, 1984.

[12] J. J. Niederhauser, M. Jaeger, M. Hejazi, H. Keppner, and M. Frenz, "Transparent ITO coated PVDF transducer for optoacoustic depth profiling," *Opt. Commun.*, vol. 253, nos. 4–6, pp. 401–406, 2005.

[13] G. Buchberger *et al.*, "Transparent, flexible, thin sensor surfaces for passive light-point localization based on two functional polymers," *Sens. Actuators A, Phys.*, vol. 239, pp. 70–78, Mar. 2016.

[14] P. C. Beard, F. Perennes, and T. N. Mills, "Transduction mechanisms of the Fabry–Perot polymer film sensing concept for wideband ultrasound detection," *IEEE Trans. Ultrason., Ferroelectr., Freq. Control*, vol. 46, no. 6, pp. 1575–1582, Nov. 1999.

[15] E. Zhang, J. Laufer, and P. Beard, "Backward-mode multiwavelength photoacoustic scanner using a planar Fabry–Perot polymer film ultrasound sensor for high-resolution three-dimensional imaging of biological tissues," *Appl. Opt.*, vol. 47, no. 4, pp. 561–577, 2008.

[16] Z. Li, A. K. Ilkhechi, and R. Zemp, "Transparent capacitive micromachined ultrasonic transducers (CMUTs) for photoacoustic applications," *Opt. Express*, vol. 27, no. 9, pp. 13204–13218, 2019.

[17] H. Li, B. Dong, Z. Zhang, H. F. Zhang, and C. Sun, "A transparent broadband ultrasonic detector based on an optical micro-ring resonator for photoacoustic microscopy," *Sci. Rep.*, vol. 4, p. 4496, Mar. 2014.

[18] E. Blumenröther, O. Melchert, J. Kanngießer, M. Wollweber, and B. Roth, "Single transparent piezoelectric detector for optoacoustic sensing—Design and signal processing," *Sensors*, vol. 19, no. 9, p. 2195, 2019.

[19] Q. Zhou *et al.*, "PMN-PT single crystal, high-frequency ultrasonic needle transducers for pulsed-wave Doppler application," *IEEE Trans. Ultrason., Ferroelectr., Freq. Control*, vol. 54, no. 3, pp. 668–675, Mar. 2007.

[20] J. M. Cannata, T. A. Ritter, W.-H. Chen, R. H. Silverman, and K. K. Shung, "Design of efficient, broadband single-element (20-80 MHz) ultrasonic transducers for medical imaging applications," *IEEE Trans. Ultrason., Ferroelectr., Freq. Control*, vol. 50, no. 11, pp. 1548–1557, Nov. 2003.

[21] Q. Zhou, K. H. Lam, H. Zheng, W. Qiu, and K. K. Shung, "Piezoelectric single crystal ultrasonic transducers for biomedical applications," *Prog. Mater. Sci.*, vol. 66, pp. 87–111, Jun. 2014.

[22] Y. Ito, K. Kushida, K. Sugawara, and H. Takeuchi, "A 100-MHz ultrasonic transducer array using ZnO thin films," *IEEE Trans. Ultrason., Ferroelectr., Freq. Control*, vol. 42, no. 2, pp. 316–324, Mar. 1995.

[23] M. Thirumoorthi and J. T. J. Prakash, "Structure, optical and electrical properties of indium tin oxide ultra thin films prepared by jet nebulizer spray pyrolysis technique," *J. Asian Ceram. Societies*, vol. 4, no. 1, pp. 124–132, 2016.

[24] *Transmittance of N-BK7 Plano-Concave Lenses, Uncoated*. [Online]. Available: https://www.thorlabs.com/newgrouppage9.cfm?objectgroup_id=2087&pn=LC1054#2089

[25] *Transmittance of UV Epoxy Norland Optical Adhesive 81*. [Online]. Available: https://www.norlandprod.com/literature/81tds.pdf

[26] W. Zou, S. Holland, K. Y. Kim, and W. Sachse, "Wideband high-frequency line-focus PVDF transducer for materials characterization," *Ultrasonics*, vol. 41, no. 3, pp. 157–161, 2003.

Cheng Fang received the B.E. degree in information engineering from Zhejiang University, Hangzhou, Zhejiang, China, in 2011, and the M.Eng. degree in electrical engineering from the Texas A&M University, College Station, TX, USA, in 2013, where he is currently pursuing the Ph.D. degree. His research interests include microfabrication technology, near-distance sensing systems, and photoacoustic imaging devices and systems.

He Hu received the B.E. degree in precision instruments and optoelectronics engineering from Tianjin University, Tianjin, China, in 2010, and the M.S. and Ph.D. degrees in electrical engineering from Texas A&M University, College Station, TX, USA, in 2012 and 2016, respectively. His Ph.D. research was focusing on micro and nano-fabrication technology and microfabricated acoustic sensors for photoacoustic microscopy (PAM). His research interests also include analog, digital, and RF IC designs, and the integration of microfabricated sensors for system-on-chip (SoC) applications.

Jun Zou (S'98–M'02–SM'15) received the Ph.D. degree in electrical engineering from the University of Illinois at Urbana-Champaign in 2002. In 2004, he joined the Department of Electrical and Computer Engineering, Texas A&M University, where he is currently a Full Professor and directs the Micro Imaging and Sensing Devices and Systems (MISDS) Lab. His current research interests lie in the development of micro and nano opto-electro-mechanical devices and systems for biomedical imaging, robotics, and artificial intelligence applications. He is a Senior Member of the SPIE, and a member of the OSA.